Sol–Gel Growth of Hexagonal Faceted ZnO Prism Quantum Dots with Polar Surfaces for Enhanced Photocatalytic Activity

Luyuan Zhang, Longwei Yin,* Chengxiang Wang, Ning Lun, and Yongxin Qi

Key Laboratory for Liquid–Solid Structural Evolution & Processing of Materials, Ministry of Education, Shandong University, Jinan 250061, China

ABSTRACT The hexagonal faceted ZnO quantum dots (QDs) about 3–4 nm have been prepared via a sol–gel route by using oleic acid (OA) as the capping agent. It is revealed by electron diffraction patterns and high resolution transmission electron microscopy lattice images that the profile surfaces of the highly crystalline ZnO QDs are mainly composed of {100} planes, with the Zn-terminated (001) faces and the opposite (00$\bar{1}$) faces presented as polar planes. Compared with spherical ZnO QDs, the hexagonal faceted ZnO QDs show enhanced photocatalytic activity for photocatalytic decomposition of methylene blue. A mechanism for the enhanced photocatalytic activity of the hexagonal faceted ZnO QDs for degradation of methylene blue is proposed. In addition to the large specific surface areas due to small size and high crystalline, the enhanced photocatalytic activity can mainly be ascribed to the special hexagonal morphology. The Zn-terminated (001) and O-terminated (00$\bar{1}$) polar faces are facile to adsorb oxygen molecules and OH^- ions, resulting in a greater production rate of H_2O_2 and $OH^\bullet$ radicals, hence promoting the photocatalysis reaction. The synthesized hexagonal-shaped ZnO QDs with high photocatalytic efficiency will find widespread potential applications in environmental and biological fields.

KEYWORDS: ZnO • quantum dots • photocatalytic activity • polar surface • microstructure • transmission electron microscopy

INTRODUCTION

The photocatalyzed degeneration of water pollutants is one of the important applications due to the requirements of sustained developments. ZnO, as a very important kind of II–VI compound semiconductors with a wide direct bandgap (3.37 eV), has found various applications in transistors (1), CO gas sensors (2), lasers (3), solar cells (4), water splitting catalysts (5), and photocatalysts (6) for decomposition of organic solution because of its specific electrical and optoelectronic properties. For the photocatalytic applications, ZnO can catalyze the generation of hydrogen peroxide effectively under UV irradiation, whereas hydrogen peroxide can decompose organic pollutants (7).

Because a photocatalytic reaction occurs at the interface between the catalyst surfaces and organic pollutants, the morphologies affecting surface atomic arrangements and coordination can play an important role in determining catalytic performance properties (8). By passivating the specific ZnO facets, thereby adjusting the growth velocity order among the ZnO facets, a variety of nanostructures, such as pyramids about 25 nm in diameter (9), nanospherical particles with a diameter of ten micrometers (10), and ellipsoids (11), have been reported. It is shown that fine-tuning of the face orientation of ZnO crystals can optimize their photocatalytic activity for H_2O_2 generation (8). The polar planes of wurtzite ZnO are very important for catalyzing N- formylation reactions (10).

ZnO quantum dots (QDs) with several nanometers in diameter and large surface to volume ratio are becoming more and more attractive due to their quantum size effect and therefore unique properties different from the bulk ZnO materials. However, the relationships between the morphology, crystal growth habit, and photocatalytic properties of the ZnO QDs with several nanometers in diameter, have not been elucidated. There is almost no report on the photocatalytic activities of hexagonal faceted ZnO QDs with only several diameters. Such speculation gives us the impetus to explore the relationship between surface orientation of ZnO QDs and their photocatalytic efficiency. Herein, we report on the hexagonal faceted ZnO quantum dots about 3–4 nm in diameter with highly faceted prisms, with high proportion of Zn-terminated (001) and O-terminated (00$\bar{1}$) polar faces and high crystallinity for enhanced photocatalytic activity. Most importantly, the presence of high proportion of polar surfaces is helpful to adsorb oxygen molecules and OH^- ions, resulting in a greater production rate of H_2O_2 and $OH^\bullet$ radicals, hence promoting the photocatalysis reaction.

EXPERIMENTAL SECTION

The ZnO QDs synthesis follows a modified sol–gel route. To obtain hexagonal faceted ZnO QDs, first zinc acetate dihydrate and a certain proportion of OA (In the experiment, the portion of Zn/OA is 1/2) were dissolved into ethanol and refluxed for 3 h at 80 °C under constant magnetic stirring. At the end of the reaction, yellowish solution was obtained. $LiOH \cdot H_2O$ with a molar ratio of [LiOH]/[Zn] = 3 was dissolved into ethanol with the help of ultrasonic stirring. Then, the above yellowish solution

* Corresponding author. E-mail: yinlw@sdu.edu.cn. Fax: 86-531-88392315. Tel: 86-531-88396970.

Received for review March 28, 2010 and accepted May 18, 2010

DOI: 10.1021/am100274d

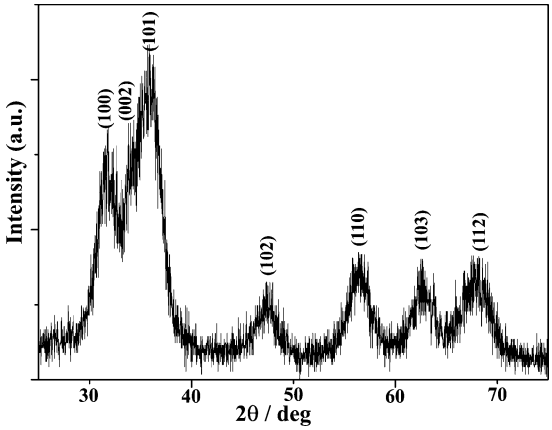

FIGURE 1. XRD pattern of prepared faceted ZnO quantum dots.

was added into the lithium hydroxide ethanolic solution, and the whole reacting system was kept at 40 °C for 1 hour under ultrasonic stirring. ZnO QDs were precipitated from the reaction system by addition of ethyl acetate or heptane. After that the products were washed with ethyl acetate and ethanol successively for several times. Nonfaceted spherical ZnO QDs were prepared without adding OA under the same experimental conditions. Hexagonal-faceted ZnO QDs grow slower than spherical ZnO QDs because of the impact of OA; therefore, to synthesize the spherical ZnO QDs with the same size, we must shorten the reaction time of spherical ZnO QDs.

X-ray powder diffraction data for the vacuum-dried ZnO products were collected on a Rigaku D/max-kA diffractometer with CuKa radiation (60 kV, 40 mA) at 25. Several drops of ZnO QDs ethanol solution were dropped onto carbon-coated copper grids to observe the microstructure. High-resolution electron microscope (HRTEM) images and electron diffraction patterns were obtained using a Phillips Tecnai 20U-Twin high-resolution transmission electron microscope operated at a 200 kV. The Fourier transform infrared (FTIR) spectrum were recorded on a Bruker Tensor27 FTIR spectrometer using KBr pellets. UV−vis absorption spectra were detected using a TU-1901 spectrophotometer and the photoluminescence (PL) spectra were measured using F-280 spectrofluorometer with an excitation wavelength of 310 nm at room temperature. The photocatalytic activity of ZnO Quantum Dots (QDs) for the decomposition of methylene blue (MB) was tested on a XPA-7 photoreactor equipped a 100 W UV lamp.

RESULTS AND DISCUSSION

Figure 1 depicts a typical X-ray diffraction pattern for the hexagonal faceted ZnO QDs. All the X-ray diffraction peaks can be indexed to (100), (002), (101), (102), (110), (103), and (112) planes of wurtzite ZnO. No other diffraction peaks related impurities can be observed. The broadening of the diffraction peaks is due to the very small particle size for the synthesized ZnO products. A typical HRTEM image is shown in Figure 2. It is shown that the synthesized ZnO QDs are highly crystalline with a unique diameter of 3−4 nm. The inset shows a Fourier transform diffraction pattern from the [001] zone axis of the single ZnO particle marked as an arrow in Figure 2a, revealing the single-crystalline nature of single ZnO QDs, and the surface of the ZnO QDs are mainly composed of {100} planes. The electron diffraction pattern in Figure 2b taken from the whole area of Figure 2a, showing the (100), (002), (101), (102), (110), and (103) diffraction rings, corresponds well with that of wurtzite ZnO. The results

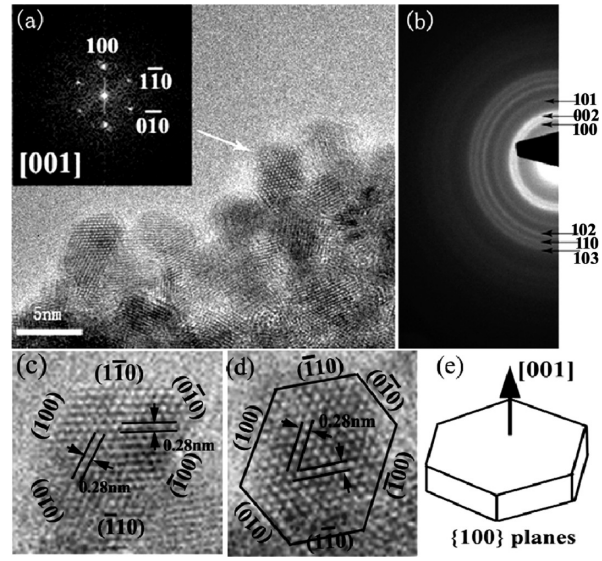

FIGURE 2. (a) HRTEM lattice image of the synthesized ZnO QDs. The left upper inset is a fast fourier transform (FFT) pattern from [001] zone axis. (b) Electron diffraction pattern from the ZnO particles in image a. (c, d) HRTEM lattice images of ZnO QDs, the 0.28 nm as illustrated corresponds well with that of *d*-spacing of (100) planes of wurtzite ZnO. (e) Illustration model for the crystal growth habit of the ZnO QDs.

from the electron diffraction patterns are in good well agreement with that of the XRD. Images c and d in Figure 2 depict typical HRTEM lattice images of two single ZnO QDs, indicating clearly the highly crystalline nature for the ZnO QDs. The ZnO QDs generally display hexagonal-shaped faceted characteristic. The 0.28 nm as illustrated in images c and d in Figure 2 corresponds well with that of *d*-spacing of {100} planes of wurtzite ZnO. It reveals that the profile surfaces of the crystalline ZnO QDs are mainly composed of the {100} plane, whereas the Zn-rich face of the hexagonal crystalline ZnO QDs particles is the (001) plane, and the opposite face is the (00$\bar{1}$) plane. Figure 2e demonstrates the crystal growth habit model of the hexagonal-like ZnO QDs. Figure 3 depicts X-ray diffraction pattern and HRTEM lattice image for the nonfaceted spherical ZnO quantum dots prepared without adding oleic acid under the same experimental conditions. The ZnO QDs are highly crystalline and 3−4 nm in diameter, but they do not display hexagonal-shaped characteristic.

The wurtzite ZnO with a polar structure can be described as hexagonal-close-packed O and Zn atoms in point group 6*mm* and space group *P*63*mc* with Zn atoms in tetrahedral sites. During ZnO QDs growth process, it is thought that "Zn_4O" tetrahedrons were first formed as "monomers", and then the monomers will aggregate to form "magic clusters" (12). Once it starts, an iterative cluster−cluster aggregation under continuous ongoing nucleation (forming of "Zn_4O" tetrahedrons and magical clusters) will occur. Because of the randomness of the aggregation, the final shape of ZnO QDs is apt to grow into spherical morphology. So, the ZnO QDs synthesized without OA are spherical. For the hexagonal faceted ZnO QDs, their growth process is modulated by OA, thus they display a different morphology. As capping agent, OA can stop the aggregation of magic clusters and hence

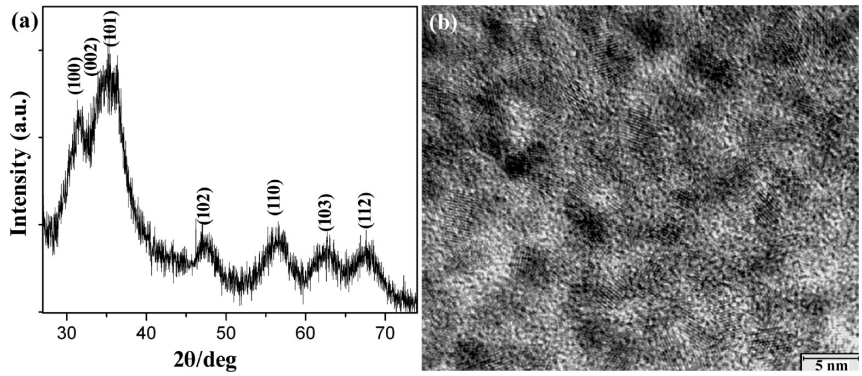

FIGURE 3. (A) XRD pattern and (b) HRTEM image of the nonfaceted spherical ZnO quantum dots.

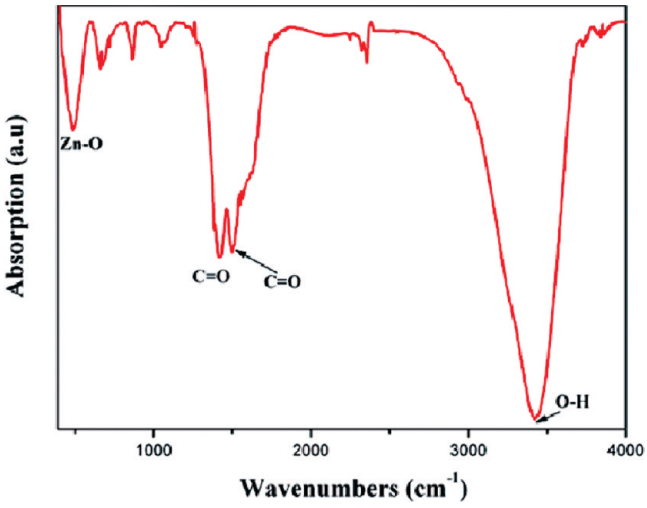

FIGURE 4. Typical Fourier transform infrared (FTIR) spectrum from the synthesized ZnO QDs.

slow the growth of ZnO. Because of an intrinsic anisotropy in the growth rate v of ZnO, the growth rate perpendicular to these faces is different: v [001] $\gg$ v [010] > v [00$\bar{1}$]. Meanwhile, earlier studies show that organic molecules like OA seem to support the preferential growth of the [001] direction (13). Hence, the ZnO QDs synthesized with OA are hexagonal faceted. From TEM analysis in Figure 2 and crystallographic view, there exist three kinds of common termination faces for the synthesized ZnO QDs, Zn-terminated (001) face, O-terminated (00$\bar{1}$) face, and {100} faces containing an equal number of Zn and O atoms (8). The (001) and (00$\bar{1}$) faces are polar, whereas the (100) face is nonpolar. Because of the coexistence of the (001), (00$\bar{1}$), and {100} faces, Zn^{2+} ions exist on the surfaces of the ZnO QDs. It is well-known that Zn^{2+} ions can covalently conjugate with OH^{-1} and carboxyl groups tightly.

Figure 4 depicts a typical Fourier transform infrared (FTIR) spectrum from the faceted ZnO QDs. In the FTIR spectrum, the peak at around 490 cm^{-1} is assigned to the Zn−O stretching (14). A broad band at 3442 cm^{-1} is also observed in the FTIR spectrum. The faceted ZnO QDs possess large surface area of {001} facets, considering the fact that the hydroxyl groups (OH^{-1}) are apt to attach on surfaces of {001} facets as discussed above, it is rationally considered that the broad band at 3442 cm^{-1} ascribed to the presence of the O−H stretching mode may be mainly

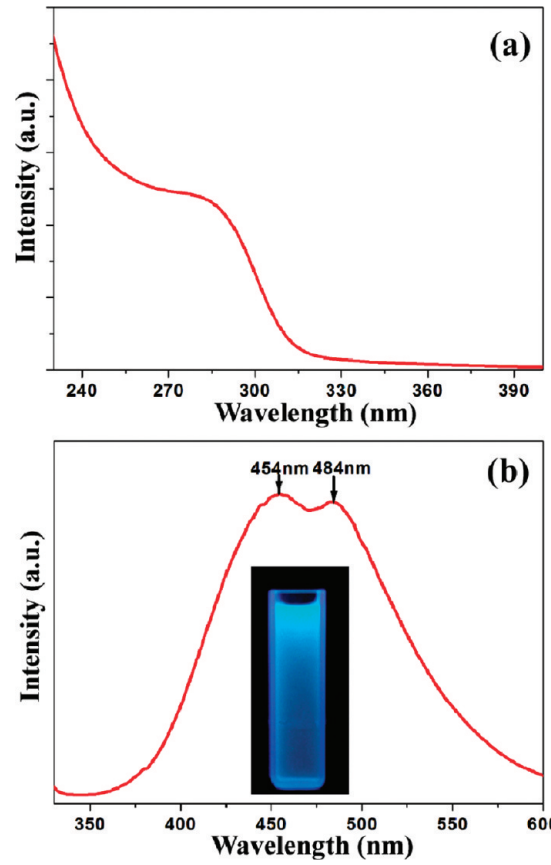

FIGURE 5. (a) UV−vis absorption spectrum, (b) photoluminescence spectrum from the faceted ZnO QDs.

resulted from the hydroxyl groups attached on surfaces of {001} facets.

Figure 5a depicts a UV−visible absorption spectrum for the faceted ZnO QDs. The wavelength of the onset of absorption is lower than that of ever reported ZnO QDs (15). It displays a position red-shift to the lower wavelength. In front of the absorption onset, a weak absorption band is observed. Figure 5b shows photoluminescence spectra of the ZnO QDs. Two emission peaks near each other centered at 454 and 484 nm are observed in the visible range, respectively. This phenomenon is different from what have been reported on ZnO QDs (15). Traditionally, there are two emission peaks emerging in the luminescence spectra of ZnO, but one emerging in ultraviolet region and the other emerging at visible region. The origin of the visible emission

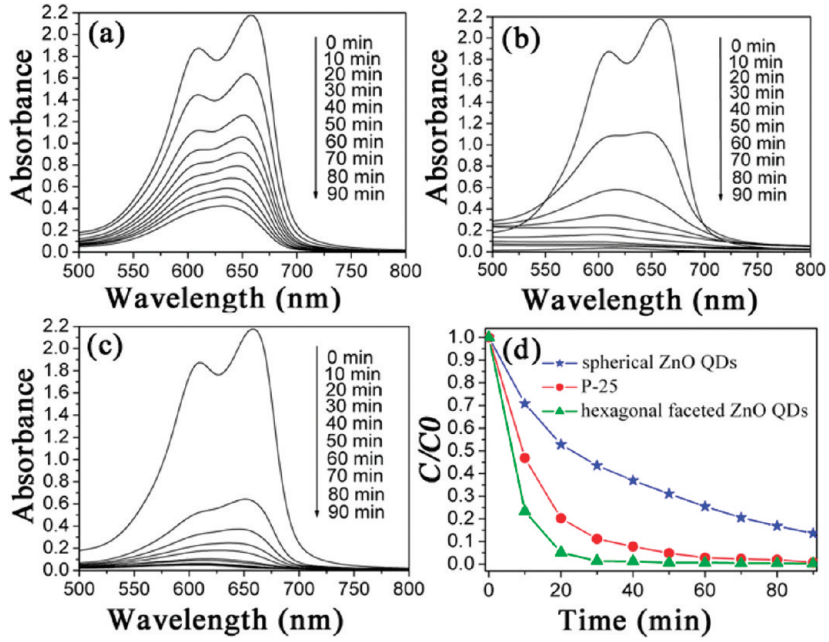

FIGURE 6. (a−c) Adsorption changes of RhB aqueous in the presence of nonfaceted spherical ZnO QDs, Degussa P-25, and hexagonal faceted ZnO QDs under irradiation with UV light at different intervals. (d) Degradation efficiency versus reaction time for all samples.

has long been debated. The visible emission is usually referred to factors such as the size, the defects, the surface, the component (16). Because of the large surface to volume ratio of ZnO QDs, most defects may exist on their surface.

Figure 6 demonstrates the photocatalytic activity of hexagonal faceted ZnO QDs. As a comparison, the photocatalytic activities of nonfaceted spherical ZnO QDs and Degussa P-25 were also tested under the same conditions. Figure 6a−c displays the time-dependent absorption spectra of methylene blue (MB) aqueous solution under UV light irradiation in the presence of the above-mentioned samples. The characteristic absorption peaks of MB at approximately 660 nm become weaker as the irradiation time increases for all samples. However, it is clearly shown that the absorption peak of MB still exists after 50 min for spherical ZnO QDs, whereas for P-25 and faceted ZnO QDs, the absorption peak nearly disappears after about 20 min of exposure. To further compare photocatalytic activities of the samples, curves of degradation efficiency versus reaction time for all samples are shown in Figure 6d. The degradation efficiency is defined as C/C_0, where C_0 and C are concentration of MB before and after the photocatalytic reaction, respectively. It is clearly indicated that the faceted ZnO QDs show the highest photocatalytic activity.

As can be revealed, the hexagonal faceted ZnO QDs show better photocatalytic performance even than that of P25. The better photocatalytic activity of the ZnO QDs can be explained by three reasons. One is that ZnO QDs possess small size and thus have large specific surface areas. As demonstrated by HRTEM and XRD, the synthesized faceted ZnO QDs are highly crystalline with a diameter of 3−4 nm. The specific surface area is a key factor influencing the photocatalytic activity and the accepted view is that the larger the specific surface area, the better the photocatalytic activity because the enhancement in specific surface area might increase the reactant adsorption (17). So, the spherical ZnO QDs have also much better photocatalytic activity. Except for their small size, the main point is that the faceted ZnO QDs display hexagonal prism structure. The most proportion of their surface are the polar faces, that is, the Zn-terminated (001) face and O-terminated ($00\bar{1}$) face. According to earlier reports, (001) face is found to be responsible for the majority of the photocatalytic activity of ZnO (18). Because of its unsaturated oxygen coordination and positive charge, (001) face is facile to adsorb oxygen molecules and OH^- ions (8). This will result in a greater rate of production of H_2O_2 and $OH^\bullet$ radicals, and hence promote the photocatalysis reaction because of their high activity to organic molecules. The third is that ZnO QDs possess more surface defects such as oxygen vacancies. These defects benefit the efficient separation of electron−hole pairs and minimize the radiative recombination of electron and hole, which produces UV emission (8). It is worth noting that in the earlier report, Ye et al. also found that the photocatalytic efficiency of ZnO is surface plane dependent (19). Ye et al. thought that the improved photocatalytic activity of polar planes is due to their stronger adsorption of organic dyes than other nonpolar planes. The photocatalytic mechanism of ZnO QDs can be generally understand as following. As ZnO is illuminated by light with energy greater than the band energy, an exciton pair is generated on the surface of ZnO, which are conduction band electrons (e^-) and valence band holes (h^+), respectively. The photoelectrons can react with oxygen when they exist on the surface of ZnO QDs, resulting in the formation of a superoxide radical anion ($O_2^{\bullet-}$). The photoinduced hole can react with surface hydroxyl to form highly reactive hydroxyl radicals ($OH^\bullet$). The superoxides and hydroxyl radicals can directly oxidize organic pullutants (16). This can be summarized by the equations.

$$ZnO + h\nu \rightarrow e^- + h^+ \quad (1)$$

$$O_2 + e^- \rightarrow O_2^{\bullet -} \quad (2)$$

$$OH^{-1} + h^+ \rightarrow OH^{\bullet} \quad (3)$$

CONCLUSIONS

In summary, the synthesized hexagonal faceted ZnO QDs about 3−4 nm in diameter show better photocatalytic performance even than that of P25. The better photocatalytic activity of the ZnO QDs can be explained by three reasons. One is that ZnO QDs possess small size and thus have large specific surface areas. The most important point is that the faceted ZnO QDs display hexagonal prism structure. The most proportion of their surface are the polar faces, that is, the Zn-terminated (001) face and O-terminated ($00\bar{1}$) face. Because of its unsaturated oxygen coordination and positive charge, (001) face is facile to adsorb oxygen molecules and OH^- ions. This will result in a greater rate of production of H_2O_2 and $OH^{\bullet}$ radicals, and hence promote the photocatalysis reaction because of their high-activity to organic molecules. The third is that ZnO QDs possess more surface defects such as oxygen vacancies.

Acknowledgment. We acknowledge support from the National Nature Science Foundation of China (Nos. 50872071 and 50972079), the Shandong Natural Science Fund for Distinguished Young Scholars (JQ200915), Nature Science Foundation of Shandong Province (Y2007F03 and Y2008F26), Foundation of Outstanding Young Scientists in Shandong Province (No. 2006BS04030), Tai Shan Scholar Foundation of Shandong Province, and Gong Guan Foundation of Shandong Province (2008GG10003019).

REFERENCES AND NOTES

(1) Goldberger, J.; Sirbuly, J. D.; Law, M.; Yang, P. *J. Phys. Chem. B.* **2005**, *109*, 9–14.
(2) Wang, J. X.; Sun, X. W.; Huang, H.; Lee, Y. C.; Tan, O. K.; Yu, M. B.; Lo, G. Q.; Kwong, D. L. *Appl. Phys. A: Mater. Sci. Process.* **2007**, *88*, 611–615.
(3) Huang, M. H.; Mao, S.; Feick, H.; Yan, H.; Wu, Y.; Kind, H.; Weber, E.; Russo, R.; Yang, P. *Science* **2001**, *292*, 1897–1899.
(4) Jiang, C. Y.; Sun, X. W.; Lo, G. Q.; Kwong, D. L.; Wang, J. X. *Appl. Phys. Lett.* **2007**, *90*, 263501.
(5) Maeda, K.; Teramura, K.; Saito, N.; Inoue, Y.; Domen, K. *J. Catal.* **2006**, *243*, 303–308.
(6) Zheng, Y.; Chen, C.; Zhan, Y.; Lin, X.; Zheng, Q.; Wei, K.; Zhu, J.; Zhu, Y. *Inorg. Chem.* **2007**, *46*, 6675–6682.
(7) Hoffmann, A. J.; Carraway, E. R.; Hoffmann, M. R. *Environ. Sci. Technol.* **1994**, *28*, 776–785.
(8) Jang, E. S.; Won, J. H.; Hwang, S. J.; Choy, J. H. *Adv. Mater.* **2006**, *18*, 3309–3312.
(9) Choi, S. H.; Kim, E. G.; Park, J.; An, K.; Lee, N.; Kim, S. C.; Hyeon, T. *J. Phys. Chem. B.* **2005**, *109*, 14792–14794.
(10) Li, G. R.; Hu, T.; Pan, G. L.; Yan, T. Y.; Gao, X. P.; Zhu, H. Y. *J. Phys. Chem. C.* **2008**, *112*, 11859–11864.
(11) Xie, R.; Li, D.; Zhang, H.; Yang, D.; Jiang, M.; Sekiguchi, T.; Liu, B.; Bando, Y. *J. Phys. Chem. B.* **2006**, *110*, 19147–19153.
(12) Spanhel, L. *J. Sol−Gel Technol.* **2006**, *39*, 7–24.
(13) Yin, M.; Gu, Y.; Kuskovsky, I. L.; Andelman, T.; Zhu, Y.; Neumark, G. F.; O'Brien, S. *J. Am. Chem. Soc.* **2004**, *126*, 6206–6207.
(14) Fernandesa, D. M.; Silvaa, R.; Hechenleitner, A. A. W.; Radovanovic, E. *Mater. Chem. Phys.* **2009**, *115*, 110–115.
(15) Spanhel, L.; Anderson, M. A. *J. Am. Chem. Soc.* **1991**, *113*, 2826–2833.
(16) Xiong, H. M.; Shchukin, D. G.; Mohwald, H.; Xu, Y.; Xia, Y. Y. *Angew. Chem. Int. Ed.* **2009**, *48*, 2727–2731.
(17) Fu, Y. S.; Du, X. W.; Kulinich, S. A.; Qiu, J. S.; Qin, W. J.; Li, R.; Sun, J.; Liu, J. *J. Am. Chem. Soc.* **2007**, *129*, 16029–16033.
(18) Lin, X.; Huang, T.; Huang, F.; Wang, W.; Shi, J. *J. Phys. Chem. B.* **2006**, *110*, 24629–24634.
(19) Ye, C.-H.; Bando, Y.; Shen, G.; Golberg, D. *J. Phys. Chem. B.* **2005**, *110*, 15146–15151.

AM100274D